pollinator service and resembles a hummingbird territory. These results are consistent with mist-net data from the same site (*20*) that show higher capture rates for territorial hummingbirds in the fragmented forest.

Subsequently, not all pasture seeds passively dropped beneath parent trees and died; many were actively transported, often hundreds of meters, to remnant forest (3.2 ha) that contained as many seedling genotypes as expected for the entire plot (38.5 ha) (*8*). Bats rarely eat in the fruiting trees where they forage. Instead they carry fruits to roosts or feeding sites in dense foliage where seeds are dropped in clusters (*21*). We frequently observed putative roosts in remnant forest as thick foliage with distinct clusters of several *S. globulifera* seedlings below, often far from any potential parent. These patterns indicate that bats loaded remnant forest with pasture seeds, fueling the preexisting reproductive imbalance.

Our findings show that the composition and performance of tropical tree subpopulations can differ among fragmented habitats. These differences can skew donorship to the gene pool. Donorship patterns also indicate shifts in the effective foraging of dispersal agents. These shifts appear to track the redistribution of food (flowers and fruits) and shelter (remnant forest) in the landscape, which further constricts the bottleneck. Notably, this feedback loop can yield abnormally high seedling densities in suboptimal habitat. These results deserve further research because mechanisms favoring some species immediately after fragmentation could determine the pool of species available for long-term forest recovery. Failure to detect such dynamics, however, could lead to mismanagement of landscapes.

References and Notes

1. T. Fleming, R. Breitwisch, G. Whitesides, *Annu. Rev. Ecol. Syst.* **18**, 91 (1987); K. S. Bawa, *ibid.* **21**, 399 (1990).
2. P. Feinsinger *et al.*, *Am. Nat.* **131**, 33 (1988); M. A. Aizen and P. Feinsinger, *Ecology* **75**, 330 (1994); *Ecol. Appl.* **4**, 378 (1994).
3. M. R. Chase, C. Moller, R. Kesseli, K. S. Bawa, *Nature* **383**, 398 (1996); J. Nason and J. L. Hamrick, *J. Hered.* **88**, 264 (1997).
4. D. A. Levin, *Am. Nat.* **145**, 109 (1995).
5. M. Ducrey, *Ann. Sci. For. Paris* **49**, 553 (1992); M. Ducrey, *ibid.* **51**, 77 (1994).
6. T. Croat, *Flora of Barro Colorado Island* (Stanford Univ. Press, Stanford, CA, 1978); V. Bittrich and M. C. E. Amaral, *Plant Syst. Evol.* **200**, 101 (1996).
7. G. Gill, R. Fowler, S. Mori, *Biotropica* **30**, 139 (1998).
8. P. R. Aldrich, J. L. Hamrick, P. Chavarriaga, G. Kochert, *Mol. Ecol.*, in press.
9. G. Daily and P. Ehrlich, *Biodivers. Conser.* **4**, 35 (1995).
10. Stems ≥2 m or ≤30 cm tall were mapped. We distinguished 66 adults from 136 saplings by dbh of the smallest flowering individual (8.5 cm). A total of 434 old seedlings were distinguished from 284 young seedlings with swollen hypocotyls. Seedlings likely antedated fragmentation (<10 years old). Sufficient DNA was retrieved for analysis from 66 adults, 137 saplings, and 413 old and 270 new seedlings.
11. T. Meagher and E. Thompson, *Ecology* **68**, 803 (1987); B. Devlin, K. Roeder, N. Ellstrand, *Theor. Appl. Genet.* **76**, 369 (1988).
12. The relative likelihood of parentage for a parent-pair on dispersed progeny, calculated with Baye's theorem, is

$$\Psi_{ijk} = \frac{\prod_{l=1}^{L} P(\delta_{kl} \mid \alpha_{il}, \alpha_{jl})}{\sum_{i=1}^{a+1}\sum_{j=1}^{a+1}\prod_{l=1}^{L} P(\delta_{kl} \mid \alpha_{il}, \alpha_{jl})} \quad (1)$$

where i and j denote a possible parents and k progeny, with α_{il}, α_{jl}, and δ_{kl} the respective genotypes (L loci). This resolves ties by fractional assignment. Gene flow from off-plot was estimated by inclusion of an $a+1$'th possible parent, g, where α_{gl} is the allele frequency. Progeny of adults that die before sampling are attributed to the pool of adults off-plot, producing an inflated gene flow estimate (a conservative bias in fragmented forest).
13. H. R. Pulliam, *Am. Nat.* **132**, 652 (1988); A. Watkinson and W. Sutherland, *J. Anim. Ecol.* **64**, 126 (1995).
14. *G* tests used numbers of selfed and outcrossed progeny assigned to adults in a habitat.
15. W. F. Laurance *et al.*, *Science* **278**, 1117 (1997).
16. S. H. Bullock and K. S. Bawa, *Ecology* **62**, 1494 (1981).
17. Lifetime reproduction (saplings and seedlings) was used to calculate N_{ev} [J. Crow and M. Kimura, *An Introduction to Population Genetics Theory* (Harper and Row, New York, 1970)]. Gene flow estimates (m) are 0.16 for fragmented forest and 0.56 for continuous forest.
18. J. Heywood, *Am. Nat.* **127**, 851 (1986).
19. S. J. Wright and C. P. van Schaik, *ibid.* **143**, 192 (1994); S. Mulkey, K. Kitajima, S. J. Wright, *Trends Ecol. Evol.* **11**, 408 (1996).
20. R. Borgella Jr., master's thesis, Cornell University, Ithaca, NY, 1995; _____ and T. Gavin, unpublished data. Hummingbird capture rates (>10, 1994 to 1997) from the same site are as follows: territorial—*Lampornis (castaneoventris) cinereicauda* (continuous/fragmented forest) = (0/41), *Amazilia tzacatl* (15/5); plastic—*Heliodoxa jacula* (4/25); trapliner—*Phaethornis guy* (53/42), *Eutoxeres aquila* (18/2); rarely territorial—*Campylopterus hemileucurus* (13/10); and uncertain—*Elvira chionura* (11/9). Behavior descriptions are from F. G. Stiles and A. F. Skutch, *A Guide to the Birds of Costa Rica* (Cornell Univ. Press, Ithaca, NY, 1989).
21. D. Levey, T. Moermond, J. Denslow, in *La Selva*, L. McDade, K. Bawa, H. Hespenheide, G. Hartshorn, Eds. (Univ. of Chicago Press, Chicago, 1994), pp. 282–294.

22. We thank P. Chavarriaga and G. Kochert for marker assistance; R. Borgella and T. Gavin for hummingbird data; and V. Apsit, M. Arnold, C. R. Carroll, J. Doebley, D. Hinrichs, W. J. Kress, J. Nason, P. Stevens, R. Wyatt, and three anonymous reviewers for discussions and comments. Field support was from L. D. Gomez, G. Hewson, R. Menjivar, and D. Biggs, Organization for Tropical Studies (OTS), and Stanford Center for Conservation. P.R.A. supported by a NSF Dissertation Improvement Grant and a NSF training grant, Sigma Xi, OTS, and University of Georgia Botany Department.

27 January 1998; accepted 27 May 1998

Interaction of Human Arp2/3 Complex and the *Listeria monocytogenes* ActA Protein in Actin Filament Nucleation

Matthew D. Welch,* Jody Rosenblatt, Justin Skoble, Daniel A. Portnoy, Timothy J. Mitchison

Actin filament assembly at the cell surface of the pathogenic bacterium *Listeria monocytogenes* requires the bacterial ActA surface protein and the host cell Arp2/3 complex. Purified Arp2/3 complex accelerated the nucleation of actin polymerization in vitro, but pure ActA had no effect. However, when combined, the Arp2/3 complex and ActA synergistically stimulated the nucleation of actin filaments. This mechanism of activating the host Arp2/3 complex at the *L. monocytogenes* surface may be similar to the strategy used by cells to control Arp2/3 complex activity and hence the spatial and temporal distribution of actin polymerization.

The pathogenic bacterium *Listeria monocytogenes* initiates actin filament polymerization at its cell surface after it gains access to the cytosol of infected host cells (*1*). Actin polymerization is tightly coupled to intracellular bacterial motility (*2*) and may provide the motile force (*3*). Thus the *L. monocytogenes* cell surface is functionally similar to the leading edge of lamellipodia in locomoting cells, where actin polymerization is linked with membrane protrusion (*4*). Understanding the mechanism by which polymerization is instigated by *L. monocytogenes* should shed light both on an essential aspect of bacterial pathogenesis and on the general mechanisms by which actin filament assembly is modulated in cells.

Actin polymerization at the *L. monocytogenes* surface is mediated by bacterial and

M. D. Welch and J. Rosenblatt, Department of Cellular and Molecular Pharmacology, University of California, San Francisco, CA 94143, USA. T. J. Mitchison, Department of Cell Biology, Harvard Medical School, Boston, MA 02115, USA. J. Skoble and D. A. Portnoy, Department of Molecular and Cell Biology and School of Public Health, University of California, Berkeley, CA 94720, USA.

*To whom correspondence should be addressed at Department of Molecular and Cell Biology, University of California, Berkeley, CA 94720, USA.

host cell factors. The only essential bacterial component is ActA (*5, 6*), a cell surface protein that recruits host cell factors that promote actin assembly. A critical host factor is the Arp2/3 complex (*7*), an evolutionarily conserved protein complex that contains actin-related proteins (Arp) in the Arp2 and Arp3 subfamilies as well as five additional proteins (*8–10*). This protein complex promotes actin assembly at the bacterial surface, mediates bacterial motility in vitro (*7*), and is localized throughout actin "comet tails" assembled by moving *L. monocytogenes* in vivo (*7, 10*). Moreover, the Arp2/3 complex is concentrated in the lamellipodia of mammalian cells (*10, 11*) and in pseudopodia of *Acanthamoeba castellanii* (*8, 12, 13*), which suggests that it is important for membrane protrusion. Genetic analysis in yeast has demonstrated that the Arp2/3 complex is essential for actin function and cell viability (*9, 14*).

To further understand the biochemical function of the Arp2/3 complex in cells, we sought to determine how it promotes actin polymerization at the *L. monocytogenes* surface. Structural models of Arp2 and Arp3 (*12*) suggest that the complex may serve as a nucleating site for the assembly of actin monomer (G-actin). Nucleation is the rate-limiting step in spontaneous actin polymerization and thus represents a kinetic barrier to actin assembly. Alternatively, the Arp2/3 complex may recruit actin filaments (F-actin) (*13*), which themselves serve as a template for polymerization. To distinguish between these mechanisms, bacteria were incubated with Arp2/3 complex and equal concentrations of rhodamine-labeled G-actin or F-actin (*15*). Actin clouds were observed surrounding bacteria incubated with Arp2/3 complex and G-actin (Fig. 1A). In contrast, no actin was associated with bacteria in the presence of Arp2/3 complex and F-actin (Fig. 1B). This strongly favors the nucleation model for Arp2/3 complex function on *L. monocytogenes*.

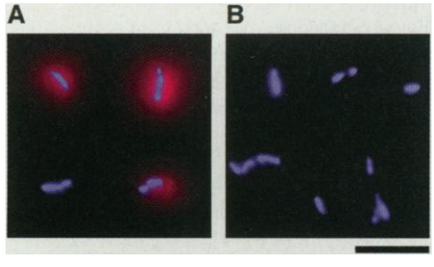

Fig. 1. Function of the Arp2/3 complex at the *L. monocytogenes* cell surface. (**A**) Composite image of DAPI-labeled *L. monocytogenes* (blue) that were incubated with 0.5 μM TMR-labeled G-actin (red) and 0.07 μM Arp2/3 complex (*15*). Between 30 and 50% of bacteria assembled actin clouds. (**B**) Composite image *L. monocytogenes* (blue) that were incubated with 0.5 μM TMR-labeled F-actin (red) and 0.07 μM Arp2/3 complex (*15*). No actin was associated with bacteria. These data represent a compilation of 17 individual experiments. Bar = 10 μm.

To determine whether the Arp2/3 complex nucleates actin polymerization in the absence of *L. monocytogenes*, we observed the effect of pure complex on the kinetics of actin assembly. Polymerization kinetics were monitored in vitro by an assay that employs pyrene-actin, a fluorescent derivative of actin that exhibits much higher intensity of fluorescence when present as F-actin than as G-actin (*16*). In this assay (*17*), actin alone exhibited typical assembly kinetics marked by an initial lag phase, indicative of the kinetic barrier to nucleation, followed by a period of rapid assembly that represents filament elongation (Fig. 2A). In the presence of the Arp2/3 complex, the kinetics of polymerization were accelerated relative to actin alone (Fig. 2A), but the initial lag phase of assembly was not significantly shortened, even at higher ratios of Arp2/3:actin. This effect on polymerization is consistent with an ability to accelerate actin filament generation by either facilitating nucleation or severing newly formed filaments. However, pure Arp2/3 complex did not affect the rate of filament depolymerization (*17*), indicating that it does not sever filaments and suggesting that it facilitates nucleation.

Actin nucleation by the Arp2/3 complex at the *L. monocytogenes* surface also requires the bacterial ActA surface protein (*7*), and synthetic peptides derived from ActA bind to G- and F-actin (*18*), which suggests that ActA may itself possess nucleating activity. To determine how ActA affects polymerization kinetics, we constructed and purified a variant of ActA called ActA-His (*19*) (Fig. 3, A and B). The kinetics of actin polymerization in the presence of ActA-His and in the absence of added protein were identical (Fig. 2C), indicating that full-length ActA does not affect actin assembly (*18*).

In addition to testing the effects of Arp2/3 complex and ActA on actin assembly individually, we monitored polymerization kinetics in the presence of both pure proteins. In the presence of Arp2/3 complex and ActA-His, the initial rate of actin assembly was accelerated up to 50-fold relative to the reactions in the presence of Arp2/3 or ActA alone (Fig. 2E). Moreover, with both factors present, the lag phase of polymerization was eliminated (Fig. 2G), indicating that Arp2/3 complex and ActA function together as a highly efficient nucleating site, which is kinetically comparable to the end of an actin filament. Addition of increasing amounts of ActA to a fixed concentration of Arp2/3 complex caused a dose-dependent acceleration of the kinetics of actin polymerization (Fig. 2H). This effect was specific to ActA-His because

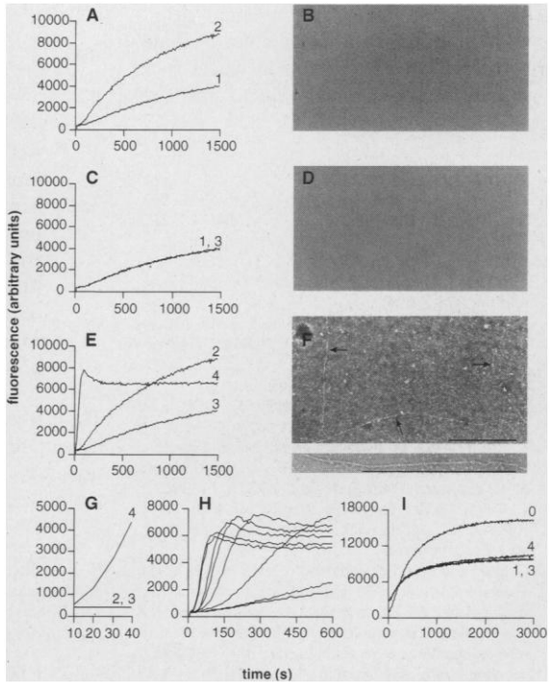

Fig. 2. Effects of the Arp2/3 complex and ActA on actin polymerization. (**A**, **C**, and **E**) Graphs of fluorescence intensity versus time after initiating polymerization in the pyrene-actin assay (*17*). Curve 1, 2 μM actin; curve 2, 2 μM actin with 30 nM Arp2/3 complex (1:65 ratio Arp2/3:actin); curve 3, 2μM actin with 30 nM ActA-His (1:65 ratio ActA:actin); curve 4, 2μM actin with 30 nM Arp2/3 complex and 30 nM ActA (1:1:65 ratio Arp2/3:ActA:actin). (**B**, **D**, and **F**) Electron micrographs of grids spotted with polymerization reaction mixtures 30 s after initiating polymerization (*21*). (B) Actin (2 μM) with 70 nM Arp2/3 complex [corresponding to (A) curve 2]. (D) Actin (2μM) with 70 nM ActA-His [corresponding to (C) curve 3]. (F) (Top) Actin (2 μM) with 70 nM ActA and 70 nM Arp2/3 complex [corresponding to (E) curve 4]. Arrows indicate actin filaments. (Bottom) Higher magnification view of an actin filament from the same reaction. Bars = 500 nm. (**G**) Expanded view of the initial 40 s of the graph in (E). (**H**) Graphs from the pyrene-actin assay. Actin (2 μM) with 20 nM Arp2/3 and, from right to left, 0, 0.04, 0.40, 4, 8, 20, 40, and 60 nM ActA-His. (**I**) Graphs from the pyrene-actin assay in the absence and presence of CD. Curve 0, 4 μM actin; curve 1, 4 μM actin with 1 μM CD; curve 3, 4 μM actin with 18 nM Arp2/3 and 1 μM CD; curve 4, 4μM actin with 18 nM Arp2/3, 10 nM ActA-His, and 1 μM CD.

addition of an unrelated protein (His-XCTK2 tail, the COOH-terminal domain of a kinesin family protein) (*20*) to the Arp2/3 complex did not accelerate polymerization kinetics relative to the Arp2/3 complex alone.

To confirm that the assembly kinetics measured by the pyrene-actin assay represented the kinetics of filament formation, we visualized filaments in polymerization reactions by electron microscopy during the lag phase of spontaneous polymerization (30 s after initiating assembly) (*21*). Filaments were observed in the reaction mixtures containing both ActA and Arp2/3 complex (Fig. 2F) but not those with Arp2/3 complex or ActA alone (Fig. 2, B and D) (*21*). These results, together with those obtained by the pyrene-actin assay, demonstrate that the Arp2/3 complex and ActA act synergistically to nucleate actin assembly. We suggest that the nucleation activity of the Arp2/3 complex is stimulated by a physical interaction with ActA because the Arp2/3 complex on its own accelerates actin polymerization, whereas ActA does not. However, we cannot rule out the possibility that ActA participates directly in nucleation.

Actin filaments in the *L. monocytogenes* comet tail are oriented with their barbed (fast growing) ends toward the bacterial surface, and barbed-end elongation is thought to drive motility (*22*). To determine which end is elongating in filaments nucleated by Arp2/3 complex and ActA, we performed the pyrene-actin assay in the presence of cytochalasin D (CD). This compound prevents

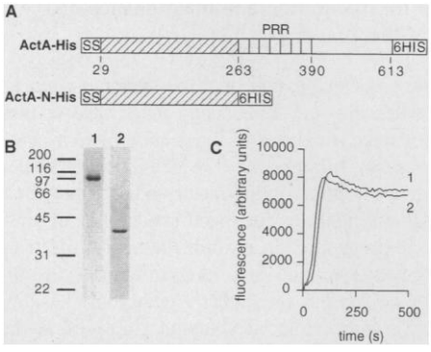

Fig. 3. ActA derivatives and their effect on actin nucleation. (**A**) Schematic representation of ActA-His and ActA-N-His (*19*) showing the signal sequence (SS), the NH_2-terminal region that is essential for actin polymerization (hatched box; amino acids 29 to 263) (*18, 24*), the central region containing four proline-rich repeats (gray boxes, PRR; amino acids 263 to 390), and the COOH-terminal tag of six histidine residues (6HIS; replaces the ActA transmembrane domain in ActA-His). (**B**) Purified ActA-His (lane 1) and ActA-N-His (lane 2) (*19*) visualized on a SDS–12% polyacrylamide gel stained with Coomassie blue. (**C**) Graphs from the pyrene-actin assay (*17*). Curve 1, 2 μM actin with 20 nM ActA-His and 20 nM Arp2/3 complex; curve 2, 2 μM actin with 20 nM ActA-N-His and 20 nM Arp2/3 complex.

assembly at barbed ends (*23*) and hence limits actin polymerization to pointed ends. When CD was included in the reaction mixture, the kinetics of Arp2/3 and ActA nucleated actin assembly were nearly identical to the kinetics in the presence of the Arp2/3 complex or actin alone (Fig. 2I). This indicates that filaments nucleated by the Arp2/3 complex and ActA elongate predominantly at their barbed ends.

We next sought to determine which domain of ActA is responsible for its activity. The NH_2-terminal region (Fig. 3A) is essential for ActA to induce actin assembly (*18, 24*). In contrast, the four proline-rich repeats in the central region (Fig. 3A) are not essential but enhance the efficiency of polymerization and motility (*24, 25*). We generated and purified ActA-N-His, which consists only of the NH_2-terminal domain of ActA (*19*) (Fig. 3, A and B). Equal amounts of ActA-N-His and ActA-His were equivalent in their ability to activate Arp2/3 complex nucleation activity in the pyrene-actin assay (*17*) (Fig. 3C). ActA-N-His alone had no effect on actin polymerization (*17*). Thus, the Arp2/3 complex interacts with the NH_2-terminal region of ActA to form a nucleating activity, and the proline-rich repeats do not contribute to nucleation in this assay. These repeats may enhance actin polymerization and bacterial motility by recruiting the Enabled/vasodilator-stimulated phosphoprotein (Ena/VASP) family of proteins (*26*) and profilin (*27*), which may promote the elongation of filaments nucleated by the Arp2/3 complex and ActA.

Our findings indicate that the Arp2/3 complex and ActA function together to nucleate actin assembly at the *L. monocytogenes* cell surface. We propose the following model for the potential role of these two proteins in actin polymerization and *L. monocytogenes* motility. Before encountering ActA, the Arp2/3 complex only weakly enhances the kinetics of actin polymerization. Upon interacting with the NH_2-terminal domain of ActA, the activity of the complex is stimulated and it nucleates actin assembly, generating actin filaments whose elongation propels the bacterium forward (*3*). Activation of the Arp2/3 complex may occur by two mechanisms. Interaction with ActA may induce a conformational change in the complex. Alternatively, the complex may be activated by self-association facilitated by ActA, which is a dimer on the bacterial surface (*28*). In either case, the ability of ActA to activate the Arp2/3 complex explains how the complex can generate actin filaments only at the bacterial surface, as is observed in vivo (*2*), although it is present throughout the actin tails assembled by moving bacteria (*7, 10*).

Activation of the Arp2/3 complex with a spatially localized factor such as ActA may represent a general strategy used to regulate the distribution of actin polymerization in cells. Cellular proteins with functions similar to ActA may recruit the complex to lamellipodia and activate its nucleating activity, leading to the generation of filaments that elongate to drive membrane protrusion. Although ActA is the only known regulator of the Arp2/3 complex, other factors such as posttranslational modification (*7, 10*) may also modulate its function. Thus, multiple pathways may operate in concert to regulate Arp2/3 complex activity. A more complete understanding of the cellular mechanisms that control actin polymerization awaits further determination of how Arp2/3-mediated nucleation is regulated and how it is integrated with other processes such as filament uncapping, elongation, cross-linking, and depolymerization.

References and Notes

1. L. G. Tilney and D. A. Portnoy, *J. Cell Biol.* **109**, 1597 (1989).
2. J. A. Theriot, T. J. Mitchison, L. G. Tilney, D. A. Portnoy, *Nature* **357**, 257 (1992); J. M. Sanger, J. W. Sanger, F. S. Southwick, *Infect. Immun.* **60**, 3609 (1992).
3. A. Mogilner and G. Oster, *Biophys. J.* **71**, 3030 (1996).
4. T. J. Mitchison and L. P. Cramer, *Cell* **84**, 371 (1996).
5. C. Kocks *et al.*, *ibid.* **68**, 521 (1992); E. Domann *et al.*, *EMBO J.* **11**, 1981 (1992).
6. G. A. Smith, D. A. Portnoy, J. A. Theriot, *Mol. Microbiol.* **17**, 945 (1995).
7. M. D. Welch, A. Iwamatsu, T. J. Mitchison, *Nature* **385**, 265 (1997).
8. L. M. Machesky, S. J. Atkinson, C. Ampe, J. Vandekerckhove, T. D. Pollard, *J. Cell Biol.* **127**, 107 (1994).
9. D. Winter, A. V. Podtelejnikov, M. Mann, R. Li, *Curr. Biol.* **7**, 519 (1997).
10. M. D. Welch, A. H. DePace, S. Verma, A. Iwamatsu, T. J. Mitchison, *J. Cell Biol.* **138**, 375 (1997).
11. L. M. Machesky *et al.*, *Biochem. J.* **328**, 105 (1997).
12. J. F. Kelleher, S. J. Atkinson, T. D. Pollard, *J. Cell Biol.* **131**, 385 (1995).
13. R. D. Mullins, W. F. Stafford, T. D. Pollard, *ibid.* **136**, 331 (1997); R. D. Mullins, J. F. Kelleher, J. Xu, T. D. Pollard, *Mol. Biol. Cell* **9**, 841 (1998).
14. E. Schwob and R. P. Martin, *Nature* **355**, 179 (1992); J. P. Lees-Miller, G. Henry, D. M. Helfman, *Proc. Natl. Acad. Sci. U.S.A.* **89**, 80 (1992); D. McCollum, A. Feoktistova, M. Morphew, M. Balasubramanian, K. L. Gould, *EMBO J.* **15**, 6438 (1996); M. K. Balasubramanian, A. Feoktistova, D. McCollum, K. L. Gould, *ibid.*, p. 6426; V. Moreau, A. Madania, R. P. Martin, B. Winsor, *J. Cell Biol.* **134**, 117 (1996); M. E. Huang, J. L. Souciet, J. C. Chuat, F. Galibert, *Yeast* **12**, 839 (1996).
15. The Arp2/3 complex was purified as described in [(*7*); M. D. Welch and T. J. Mitchison, *Methods Enzymol.* **298** (1998)]. Actin was purified [J. A. Spudich and S. Watt, *J. Biol. Chem.* **246**, 4866 (1971)], labeled with *N*-hydroxysuccinimidyl 5-carboxytetramethylrhodamine (TMR) [D. R. Kellogg, T. J. Mitchison, B. M. Alberts, *Development* **103**, 675 (1988)], and stored in G-buffer [5 mM tris-HCl (pH 8.0), 0.2 mM $CaCl_2$, 0.2 mM adenosine triphosphate (ATP), 0.2 mM dithiothreitol (DTT)]. Monomeric TMR-labeled actin was isolated by centrifuging actin in G-buffer at 228,000*g* for 15 min to remove filaments. TMR-labeled actin filaments were polymerized by adding tris-HCl (pH 8.0) to 50 mM and NaCl to 50 mM and isolated by centrifugation through an F-buffer cushion [50 mM NaCl, 50 mM tris-HCl (pH 8.0), 0.2 mM DTT, 0.5 mM ATP] at 228,000*g* for 15 min. Equal concentrations of G- and F-actin (0.5 μM) were incubated with Arp2/3 complex (0.3 to 0.5 μM) and 4′,6-diamidino-2-phenylindole (DAPI)–labeled *L. monocytogenes* strain SLCC-5764 as described [(*7*); M. D. Welch and T. J. Mitchison, *Methods Enzymol.* **298** (1998)]. The mix was squashed between a glass slide and coverslip and

incubated at 22°C for 20 min before it was viewed by fluorescence microscopy.
16. T. Kouyama and K. Mihashi, *Eur. J. Biochem.* **114**, 33 (1981); J. A. Cooper, S. B. Walker, T. D. Pollard, *J. Muscle Res. Cell Motil.* **4**, 253 (1983).
17. The pyrene-actin assay measures the weight concentration of polymer over time and is not sensitive to the distribution of filament lengths (*16*). Pyrene-actin was prepared as described in (*16*). Pyrene-labeled G-actin and unlabeled G-actin were isolated by centrifuging actin in G-buffer at 228,000*g* for 15 min to remove F-actin. For polymerization reactions, the Arp2/3 complex, ActA-His, and/or ActA-N-His were mixed and brought to 5 μl in control buffer [20 mM Mops (pH 7.0), 100 mM KCl, 2 mM $MgCl_2$, 5 mM EGTA, 1 mM EDTA, 0.2 mM ATP, 0.5 mM DTT, 10% (v/v) glycerol]. This solution was immediately mixed with 5 μl of 10× initiation buffer (20 mM $MgCl_2$, 10 mM EGTA, 5 mM ATP) and immediately added to 40 μl of G-actin solution (90% unlabeled actin and 10% pyrene-actin in G-buffer) to initiate polymerization. To monitor actin depolymerization, 7 μM pyrene G-actin was polymerized for 4 to 5 hours at 20°C by adding 10× initiation buffer (20 mM $MgCl_2$, 10 mM EGTA, 5 mM ATP). Depolymerization was initiated by diluting 2 μl of F-actin into 48 μl of G-buffer containing 1 μl of control buffer or 1 μl of 6.4 μM Arp2/3 complex in control buffer (0.27 μM actin, 0.13 μM Arp2/3). Pyrene fluorescence was monitored with a fluorometer (excitation wavelength, 365 nm; emission wavelength, 407 nm).
18. I. Lasa *et al.*, *EMBO J.* **16**, 1531 (1997).
19. To generate ActA-His, a truncated *actA* gene encoding amino acids 1 to 613 but lacking the transmembrane domain was amplified by polymerase chain reaction (PCR). Primers used were GGAAGCTTGTGGATGCTTCTGAAAGTGAC (upstream of the *actA* promoter) and GGGGATCCCGTCGTATGGTTCCCTGG (bases 1812 to 1839 of *actA*; Bam HI site is underlined). The PCR product was digested with Bam HI and Hin dIII (site upstream of promoter) and was subcloned into pAM401, yielding pDP2683. To introduce the His_6 tag, the Bam HI–Xba I fragment of pQE-60 (Qiagen) encoding amino acids GSRSHHHHHH (G, Gly; S, Ser, R, Arg; H, His) was subcloned into pDP2683 to yield pDP2717. This was transformed into *L. monocytogenes* strain DPL1545 (*6*) to yield strain DPL2723. To generate ActA-N-His, a fragment of *actA* encoding amino acids 1 to 263 was amplified by PCR. Primers used were CGGGATCCTGAAGCTTGGGAAGCAG (upstream of *actA* promoter; Bam HI site underlined) and GCTCTAGATTAGTGGTGGTGGTGGTGCGAAGCATTTACCTCTTCACT (bases 769 to 789 of *actA*; Xba I site underlined), which encodes the His_6 tag. The PCR product was digested with Bam HI and Xba I and ligated into pAM401 to yield pDP3624. This was transformed into *L. monocytogenes* strain DPL1545 to yield strain DPL3625. Secreted ActA-His and ActA-N-His were purified from culture media; 475 ml of brain heart infusion media containing chloramphenicol (10 μg/ml) (BHI cm10) was inoculated with 25-ml overnight cultures of strain DPL2723 or DPL3625 in BHI cm10 and was grown at 37°C for 6 to 8 hours. After bacteria were pelleted, protein was precipitated from the supernatant by adding ammonium sulfate to 40% (ActA-His) or 60% (ActA-N-His) saturation. Precipitated protein was resuspended in binding buffer [20 mM Mops (pH 7.0), 100 mM KCl, 20 mM imidazole (pH 7.0)] and bound to 0.5 ml of nickel nitrilotriacetic acid (Ni-NTA) agarose resin (Qiagen). The resin was washed with binding buffer and proteins were eluted with elution buffer [20 mM Mops (pH 7.0), 100 mM KCl, 250 mM imidazole (pH 7.0)]. Eluted proteins were further purified by Superose-6 (Pharmacia) gel-filtration chromatography in control buffer for the pyrene-actin experiments (*17*) and were frozen in $N_2(l)$ and stored at −80°C.
20. C. E. Walczak, S. Verma, T. J. Mitchison, *J. Cell Biol.* **136**, 859 (1997). His-XCTK2 tail alone (20 nM) had no effect on the polymerization of 2 μM actin in the pyrene-actin assay (*17*).
21. For electron microscopy, ActA-His (70 nM) and/or Arp2/3 complex (70 nM) were mixed with 10 μl of 2× polymerization buffer [100 mM KCl, 20 mM imidazole (pH 7.0), 2 mM EGTA, 2 mM $MgCl_2$] and immediately added to 10 μl of 5 μM G-actin (in G-buffer containing 0.5 mM ATP). After polymerizing for 30 s, 2 μl of actin mix was spotted onto Formvar-coated glow-discharged grids (Pellco), washed with 1× polymerization buffer and distilled H_2O, and negatively stained with 1% uranyl acetate in 50% methanol. At higher actin concentrations or longer polymerization times, some filaments were observed in all reaction mixtures, although more filaments were consistently observed in reaction mixtures containing both the Arp2/3 complex and ActA.
22. L. G. Tilney, D. J. DeRosier, M. S. Tilney, *J. Cell Biol.* **118**, 71 (1992); L. G. Tilney, D. J. DeRosier, A. Weber, M. S. Tilney, *ibid.* p. 83.
23. J. A. Cooper, *ibid.* **105**, 1473 (1987).
24. S. Pistor, T. Chakraborty, U. Walter, J. Wehland, *Curr. Biol.* **5**, 517 (1995); I. Lasa, V. David, E. Gouin, J. B. Marchand, P. Cossart, *Mol. Microbiol.* **18**, 425 (1995).
25. G. A. Smith, J. A. Theriot, D. A. Portnoy, *J. Cell Biol.* **135**, 647 (1996).
26. T. Chakraborty *et al.*, *EMBO J.* **14**, 1314 (1995); F. B. Gertler, K. Niebuhr, M. Reinhard, J. Wehland, P. Soriano, *Cell* **87**, 227 (1996); M. Reinhard *et al.*, *EMBO J.* **14**, 1583 (1995).
27. J. A. Theriot, J. Rosenblatt, D. A. Portnoy, C. P. Goldschmidt, T. J. Mitchison, *Cell* **76**, 505 (1994); J. B. Marchand *et al.*, *J. Cell Biol.* **130**, 331 (1995).
28. P. Mourrain *et al.*, *Proc. Natl. Acad. Sci. U.S.A.* **94**, 10034 (1997).
29. We are indebted to G. Smith for help and advice on generating secreted derivatives of ActA. We thank M. Moritz and C. Walczak for comments on the manuscript. Supported by grants from the NIH to T.J.M. (GM48027) and D.A.P. (AI26919). M.D.W. is a Leukemia Society of America Special Fellow.

1 April 1998; accepted 29 May 1998

Congenital Heart Disease Caused by Mutations in the Transcription Factor *NKX2-5*

Jean-Jacques Schott,* D. Woodrow Benson,*† Craig T. Basson,‡ William Pease, G. Michael Silberbach, Jeffrey P. Moak, Barry J. Maron, Christine E. Seidman, J. G. Seidman§

Mutations in the gene encoding the homeobox transcription factor NKX2-5 were found to cause nonsyndromic, human congenital heart disease. A dominant disease locus associated with cardiac malformations and atrioventricular conduction abnormalities was mapped to chromosome 5q35, where *NKX2-5*, a *Drosophila tinman* homolog, is located. Three different *NKX2-5* mutations were identified. Two are predicted to impair binding of NKX2-5 to target DNA, resulting in haploinsufficiency, and a third potentially augments target-DNA binding. These data indicate that NKX2-5 is important for regulation of septation during cardiac morphogenesis and for maturation and maintenance of atrioventricular node function throughout life.

Cardiac development is a complex biological process requiring the integration of cell commitment, morphogenesis, and excitation-contraction coupling (*1, 2*). Several transcription factors (*3*) have been implicated in this process on the basis of their spatial and temporal patterns of expression or their phenotypic effects when they are functionally inactivated in flies or mice. Analyses of the *tinman* gene in *Drosophila melanogaster*, which encodes a homeobox transcription factor, indicate that it has an essential role for specification of heart muscle progenitors in nascent mesoderm (*4*). Targeted disruption of a murine homolog of *tinman*, *Nkx2.5*, causes early embryonic lethality (*5*), with cardiac development arrested at the linear heart tube stage, prior to looping. Cardiac expression of *Nkx2.5* continues throughout development and into adult life (*6*), but the functions regulated by its continued expression are unknown.

Identification of human mutations that cause congenital heart disease offers a complementary approach to gene ablation studies and particularly fosters definition of gene defects that perturb later stages of cardiac development. Cardiac septation is a critical morphogenetic process in which the primordial single atrium and ventricle are partitioned into four chambers. Mistakes in this process occur commonly in humans; 1 in 1500 live births have an atrial septal defect

J.-J. Schott and J. G. Seidman, Department of Genetics and Howard Hughes Medical Institute, Harvard Medical School, Boston, MA 02115, USA. D. W. Benson, C. T. Basson, C. E. Seidman, Cardiovascular Division and Howard Hughes Medical Institute, Brigham and Women's Hospital, Boston, MA 02115, USA. W. Pease, Harrisburg Hospital, Harrisburg, PA 17104, USA. G. M. Silberbach, Division of Pediatric Cardiology, Oregon Health Science University, Portland, OR 97201, USA. J. P. Moak, Division of Pediatric Cardiology, Children's National Medical Center, Washington, DC 20010, USA. B. J. Maron, Minneapolis Heart Institute Foundation, Minneapolis, MN 55407, USA.

*These authors contributed equally to this work.
†Present address: Cardiovascular Genetics, Medical University of South Carolina, Charleston, SC 29451, USA.
‡Present address: Cardiovascular Division, Cornell University Medical College, New York, NY 10021, USA.
§To whom correspondence should be addressed. E-mail: seidman@rascal.med.harvard.edu